1-1-2009

Hot ductility of Nb- and Ti-bearing microalloyed steels and the inlfuence of thermal history

Kristin R. Carpenter
University of Wollongong, kristinc@uow.edu.au

Rian J. Dippenaar
University of Wollongong, rian@uow.edu.au

Chris Killmore
BlueScope Steel, Wollongong

Hot Ductility of Nb- and Ti-Bearing Microalloyed Steels and the Influence of Thermal History

K.R. CARPENTER, R. DIPPENAAR, and C.R. KILLMORE

The hot ductility of Nb, Ti, and Nb-Ti containing steels has been studied under direct-cast conditions. A Gleeble 3500 thermomechanical simulator was used to determine hot ductility over the temperature range 1100 °C to 700 °C at a low strain rate of 7.5×10^{-4} s^{-1}. Tensile samples were cooled at two different cooling rates, 100 °C/min and 200 °C/min, simulating, respectively, thick and thin slab casting processes. Complex thermal patterns designed to simulate the cooling conditions experienced near the surface of a slab during continuous casting were carried out for the Nb-Ti steel. The Nb-Ti steel had lower ductility than both the Nb and Ti steels. Increasing the cooling rate generally deteriorated ductility. The low recovery of ductility at higher temperatures is explained in terms of a low strain rate and fine precipitation delaying the onset of dynamic recrystallization. This can promote intergranular cracking as a result of grain boundary sliding in the austenite. At lower temperatures, ductility was further reduced due to the formation of thin ferrite films at the prior austenite grain boundaries. Simulating the thermal history experienced near the surface of thin (90 mm) cast slab improved ductility of the Nb-Ti steel by promoting coarser NbTi(C,N). This exposes a potential flaw in a simplified hot-ductility test: a failure to accurately represent the influence of the thermomechanical schedule on precipitation and, hence, hot ductility.

DOI: 10.1007/s11661-008-9749-1

I. INTRODUCTION

THE simple hot-tensile test has been found to be useful in assessing the likelihood that steel will develop transverse surface cracks during the straightening operation in the continuous casting process.[1–4] However, for such a test to have relevance in practice, it is imperative that the thermal history of the surface of a slab that is subjected to straightening be simulated as accurately as possible in the laboratory hot tensile tests. It is therefore more appropriate to use tensile specimens that have been melted *in situ* (direct cast structures) than specimens that have been reheated to the test temperature.[1,5,6] It is specifically important to use *in-situ* melting of tensile specimens to evaluate hot ductility of steels containing Ti and S.[5–7] In these steels, *in-situ* melting ensures complete resolution of Ti and sulfide particles and provides a segregated, coarse-grained microstructure similar to that observed in continuous casting practice.

Commercially, small additions of Ti have been found to reduce the propensity to crack formation during the straightening operation in continuous casting of steel slabs.[4,6–8] However, *in-situ* melted laboratory tensile tests generally show that Ti has little or even an adverse effect on hot ductility and it is alleged that precipitation of fine TiN or Nb-Ti(C,N) particles during laboratory tests accounts for the detrimental effect of Ti on hot ductility.[2,6,9,10] This apparent discrepancy between laboratory and commercial findings could possibly be accounted for by the fact that the laboratory specimen is subjected to a very simple cooling cycle, whereas the surface of a slab experiences a very complex cooling cycle prior to straightening and, hence, a very different precipitation sequence of carbonitrides.[2,6,9,10] Therefore, it is important to simulate as accurately as possible the thermal history of the near-surface region of continuously cast slabs in laboratory tests.

The present investigation compares the hot ductility, determined following *in-situ* melting, of Nb, Ti, and Nb-Ti containing low alloy steels, cooled at rates of 100 °C/min and 200 °C/min, thus simulating the cooling conditions of conventional and thin slabs, respectively. A major difference between conventional and thin-slab casting is the significantly shorter solidification time (~22.5 minutes for 250-mm-thick slab and 2.5 minutes for 80-mm-thick slab) and faster cooling rates for the thinner slabs. The different thermal history of the surface of the slab between conventional and thin slab casting can profoundly effect precipitation and, thus, hot ductility. Consequently, the influence of thermal history, based on thin-slab casting, on hot ductility of the Nb-Ti steel was assessed.

K.R. CARPENTER, Development Metallurgist, formerly with the School of Mechanical, Materials and Mechatronics, University of Wollongong, is with BlueScope Steel, Flat Products. Contact e-mail: kristin.carpenter@bluescopesteel.com R. DIPPENAAR, Head of Postgraduate Studies, is with the School of Mechanical, Materials and Mechatronics, University of Wollongong, Wollongong NSW 2522, Australia. C.R. KILLMORE, Product Design Manager, is with BlueScope Steel, Flat Products, Port Kembla NSW 2505, Australia.
Manuscript submitted May 6, 2008.
Article published online January 21, 2009

II. EXPERIMENTAL

The compositions of the steels used in this study are shown in Table I. The Nb steel was a strip grade for structural tubing applications, and the two Ti-bearing steels were plate grades. Samples were cut from 250-mm-thick continuously cast slab and were machined with their axes parallel to the casting direction, 115 mm in length and 10 mm in diameter. A Gleeble 3500 thermomechanical simulator (Dynamic Systems Inc., Poestenkill, NY) was used to conduct hot tensile testing at the University of Wollongong, Australia.

Figure 1 displays the thermomechanical treatment imposed on the hot tensile tests. Figure 1(a) shows the direct-cast procedure (pattern I), while Figure 1(b) shows more complex thermal cycles designed to better simulate thermal temperature oscillations encountered in practice (pattern II). In pattern I (Figure 1(a)), the central part of a specimen is melted, and in order to compensate for shrinkage during solidification, a compressive deformation of ~7 pct is applied during cooling from the melting temperature to 1370 °C at a rate of 360 °C/min. The specimen is then cooled at a rate of either 100 °C/min or 200 °C/min to the test temperature (between 700 °C and 1100 °C). In pattern II (Figure 1(b)), a similar melting procedure is followed, but the specimen is cooled at a rate of 1200 °C/min to 900 °C (T_{min}). Following cooling to T_{min}, three different thermomechanical cycles were imposed. In cycles 1 and 2, a specimen is heated from T_{min} to 1100 °C (T_{max}) at a rate of 200 °C/min and then cooled to the test temperature (T_{test}) of 900 °C, at an average cooling rate of 200 °C/min. Temperature oscillations were introduced on cooling from 1100 °C to the test temperature of 900 °C. The amplitude of oscillations was ±50 °C with a period of 30 seconds for cycle 1 and ±100 °C with a period of 60 seconds for cycle 2. For cycle 3, the amplitude of oscillations was ±50 °C, but with an average cooling rate of 100 °C/min from T_{min} to T_{test}.

The key temperatures used in pattern II were selected from the cooling profile of the near surface region of a 90-mm-thick, commercially cast slab.[16] The surface temperature of a cast slab drops sharply on exiting the mold but, subsequently, is reheated due to the conduction of heat from the hot central region of the slab. Following this, thermal oscillations, during cooling to the straightening segment, are introduced due to the alternating impingement of water sprays and guide rolls on the slab.

Quartz tubes with a diametrical clearance of 0.2 mm were used to contain the molten zone in the center of the tensile specimen. Samples were held for 1 minute at the test temperature and then strained to failure at a rate of approximately 7.5×10^{-4} s^{-1}, followed by an immediate water quench.

Table I. Chemical Compositions of Steels (Weight Percent) and Calculated Ar_3 Temperature

Alloy	C	Mn	S	Al	Nb	Ti	N	Ar_3 (°C)	Ae_3 (°C)
Nb steel	0.155	0.73	0.013	0.036	0.022	<0.003	0.0033	763.9	823.7
Ti steel	0.165	1.11	0.012	0.033	<0.001	0.018	0.0027	731.9	826.3
Nb-Ti steel	0.160	1.23	0.017	0.027	0.019	0.015	0.0031	726.4	827.8

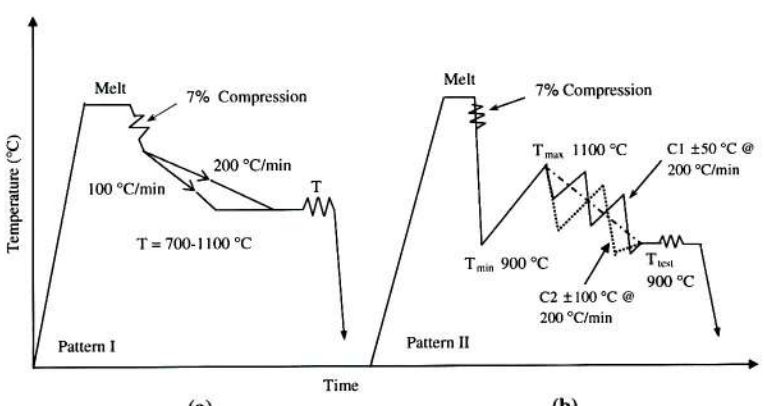

Fig. 1—Thermal patterns used in the hot-tensile tests: (*a*) Pattern I (no thermal oscillations). (*b*) Pattern II with three different thermal oscillations: C1 ± 50 °C at 200 °C/min, C2 ± 100 °C at 200 °C/min, and C3 ± 50 °C at 100 °C/min (not shown).

Metallographic examinations were carried out on longitudinal sections of the tensile specimen, taken close to the point of fracture. After optical examination, the specimens were repolished and lightly etched in 2.5 pct Nital in preparation for carbon coating. To ensure carbon replicas were taken from adjacent to the fracture face, only the area adjacent to the fracture face was exposed for carbon coating. Specimens were then placed in 5 pct hydro-bromic acid to strip the replicas, which were washed in two baths of ethanol, then floated for collection on copper grids in a mixture of 80 pct distilled water and ethanol. Carbon extraction replicas were examined in a PHILIPS* CM200 transmission electron microscope (TEM) equipped with EDS. Fracture surfaces were examined with a JEOL** JEM-3000 scanning electron microscope (SEM) with an LaB6 gun.

*PHILIPS is a trademark of Philips Electronic Instruments Corp., Mahwah, NJ.

**JEOL is a trademark of Japan Electron Optics Ltd., Tokyo.

III. RESULTS

Figures 2(a) through (c) show the hot-ductility curves (percent reduction in area (RA) as a function of test temperature) for specimens subjected to pattern I treatment. In the industrially important temperature range 800 °C to 900 °C, there is very little difference in the hot ductility of the three steels, and in all three cases, the ductility drops from about 20 pct at 900 °C to about 10 pct at 800 °C. Both the Nb steel and the Ti steel have a ductility minimum at 800 °C, but there is a significantly higher ductility recovery in the Ti-containing steel compared to the Nb-containing steel when the test temperature is dropped from 800 °C to 700 °C. By comparison, the Nb-Ti steel has a ductility minimum at 750 °C and recovers some of the ductility at the lower test temperature of 700 °C. At test temperatures exceeding 900 °C, the Nb steel is more ductile than the Ti steel. The Nb-Ti steel displayed a sharp drop in ductility between 1025 °C and 950 °C, particularly at the higher cooling rate. This phenomenon was not observed in the other steels. An increase in the cooling rate caused a marginal reduction in ductility in all three steels at the high-temperature end of the ductility trough.

A comparison of the hot ductility at 900 °C of the Nb-Ti steel treated through patterns I and II respectively, is shown in Figure 3. It follows that the introduction of thermal oscillations prior to hot-tensile testing improved the hot ductility of the Nb-Ti steel.

In specimens that displayed minimum ductility, thin bands of proeutectoid ferrite formed on austenite grain boundaries, as typically shown in Figure 4. In Figure 4, thin films of ferrite decorated the prior austenite boundaries in a Nb steel, tested at 800 °C. Thin films

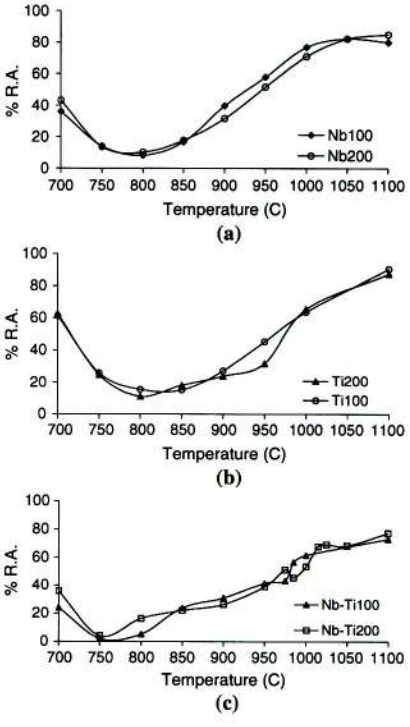

Fig. 2—Hot-ductility curves for tests conducted using pattern I where (*a*) Nb steel, (*b*) Ti steel, and (*c*) Nb-Ti steel. Cooling rates were 100 °C/min and 200 °C/min, respectively.

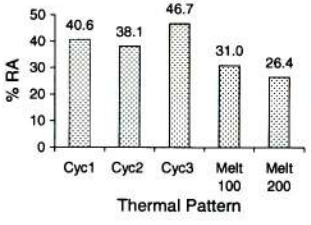

Fig. 3—RA at a test temperature of 900 °C for the Nb-Ti steel. Pattern II, cycles 1 through 3, is compared to pattern I. The cooling rates were 100 °C/min and 200 °C/min, respectively.

of deformation-induced ferrite have been shown to be able to form up to the Ae_3 temperature,[17,18] which was calculated using Andrew's formula[19] to be just above

Fig. 4—Typical optical micrograph showing thin films of ferrite decorating the prior austenite boundaries, Nb steel, test temperature, 800 °C.

820 °C (Table I). At test temperatures below 750 °C, larger volume fractions of ferrite formed.

The SEM analysis revealed that the fracture surface just below the Ar_3 temperature displayed a mixture of microvoid coalescence and intergranular decohesion. In microvoid coalescence, voids initiated during staining, predominately at inclusions or precipitates at grain boundaries, link up until intergranular failure results. As the name of the mechanism suggests, microvoid coalescence is characterized by small ductile dimples on the fracture surface. An example of intergranular failure *via* microvoid coalescence is shown in Figure 5(a). Fracture surfaces obtained from specimens tested in the single-phase austenite region exhibited intergranular decohesion, displaying flat, featureless facets, indicating failure due to grain boundary sliding.[9,12] An example of such a failure is shown in Figure 5(b). Large, deep voids were observed in specimens that displayed high ductility (not shown).

In the Ti steel, large TiN precipitates, 50 to 250 nm, predominantly cubic or rectangular in shape, were found with increasing regularity the higher the test temperature was, suggesting these particles predominately formed during testing and not during resolidification. Fine, <30 nm, spherical TiN precipitates formed below 1000 °C. The mean equivalent diameter was used to measure particle size in order to account for the unsymmetrical globular particles and to standardize the measurement technique. The mean equivalent diameter and the number of particles counted for the Nb steel and Nb-Ti steel as a function of thermal history are summarized in Table II. Video-Pro image analysis software was used to measure the particles to an accuracy of 0.5 μm.

In the Nb steel, fine (<30 nm) spherical, Nb-containing precipitates were detected in specimens tested between 950 °C and 875 °C at a cooling rate of 100 °C/min and between 850 °C and 750 °C at a cooling rate of 200 °C/min. This steel also contained spherical- or globular-shaped Nb(C,N) precipitates. Larger precipitates (>50 nm) were found in specimens tested above

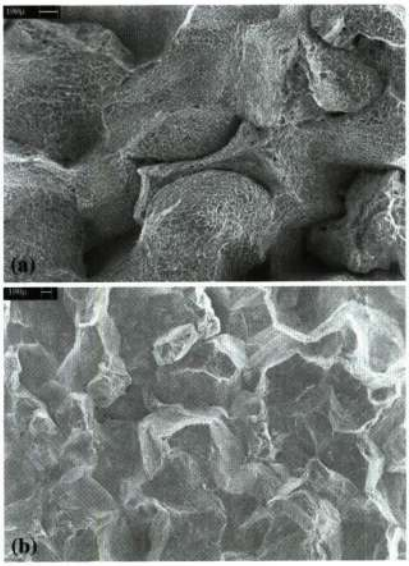

Fig. 5—(*a*) Dimpled fracture surface, test temperature 750 °C, showing typical mixed intergranular failure *via* microvoid coalescence in the Ti-steel. (*b*) Fracture surface, test temperature 800 °C, displaying intergranular failure with flat featureless facets, typical of grain boundary sliding in the Nb steel.

Table II. Summary of the Mean Equivalent Diameter and Count, as a Function of Thermomechanical Treatment, for the Nb-Ti and Nb Steels

Steel	Thermomechanical Condition	Test Temperature (°C)	Equivalent Diameter (nm)	Count
Nb-Ti	pattern 1	1000	42.8	22
	100 K/min	985	26.4	100
		950	11.4	60
		900	5.2	840
		850	4.7	100
Nb-Ti	pattern 1	1000	23.6	273
	200 K/min	975	29.0	48
		950	12.2	199
		900	5.8	332
		850	4.1	245
Nb	pattern 1	950	27.2	20
	100 K/min	900	13.4	107
		850	4.9	111
Nb	pattern 1	950	7.7	96
	200 K/min	900	6.4	90
		850	6.2	47
		900	4.6	184
		850	5.1	74

900 °C. Specimens tested between 800 °C and 700 °C contained few precipitates, but several MnS inclusions were observed.

For the Nb-Ti steel, EDS confirmed the presence of Nb, Ti, and N in almost all particles, indicating mixed Nb-Ti carbonitrides, presumably NbTi(C,N). In specimens tested between 950 °C and 900 °C, larger TiN particles were also present. Precipitates smaller than 30 nm were found in specimens tested at temperatures up to 1000 °C, and they were slightly finer when the higher cooling rate was used. Precipitates of the cruciform morphology were also found at testing temperatures of 1000 °C and above in specimens subjected to pattern I treatment.

Histograms of precipitate distributions for pattern II, cycles 1 through 3 for the Nb-Ti steel, are shown in Figures 6(a) through (c). Figure 6(d) shows the histogram for specimens subjected to pattern I treatment, test temperature 900 °C, and cooling rate 200 °C/min. (Note the change in scale between Figures 6(a) through (d)). Inspection of the histograms (Figures 6(a) through (d)) reveals that much coarser precipitates formed under cyclic temperature oscillations, compared to the simple pattern I treatment.

Figure 7 shows that the RA in the hot-ductility test is increased by an increase in the size of carbonitride precipitates when tests are conducted in the single-phase

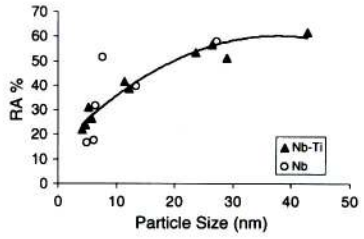

Fig. 7—RA as a function of carbonitride precipitate mean diameter in the Nb and Nb-Ti steels in the single-phase austenite region.

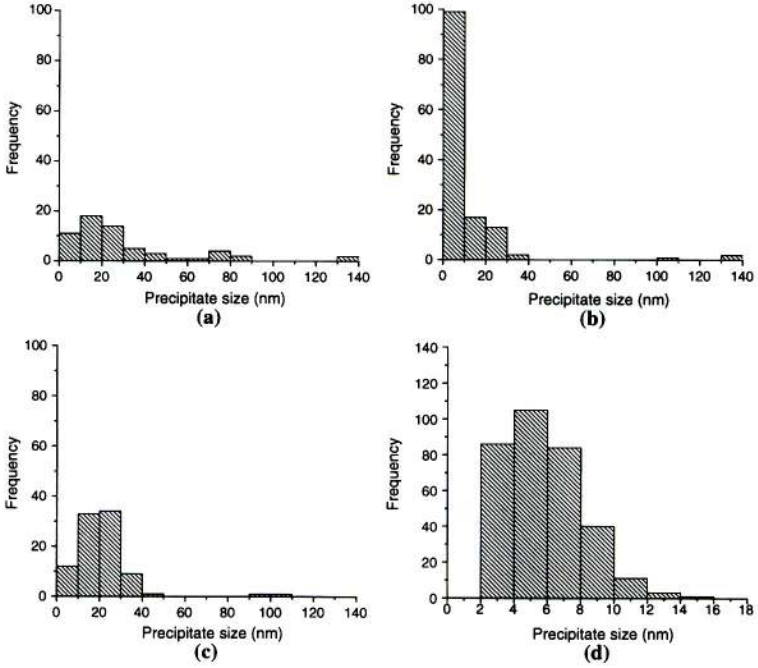

Fig. 6—Histograms of precipitate distributions in the Nb-Ti steel. Test temperature 900 °C where (*a*) through (*c*) pattern II, cycles 1 through 3, and (*d*) pattern I, cooling rate 200 °C/min. (Note the different scale in Fig. 5(d).)

austenitic region. However, it is interesting to note that hot ductility is a sharp function of precipitate particle size in the range 5 to 15 nm, but an increase in precipitate size beyond 15 nm does not seem to have a significant influence on hot ductility. It is well established that grain boundary sliding is enhanced by precipitation of fine particles,[4] and hence, grain boundary sliding can in large measure be circumvented by particle coarsening. This finding has important practical significance and will be discussed further in Section IV.

IV. DISCUSSION

In accordance with currently accepted theory,[1,3,4,6] minimum ductility for all the steels investigated is found when a thin ferrite film forms on austenite grain boundaries, as shown in Figure 4. Thermo-Calc was used to determine the Ar_3 temperatures, as included in Table I. The higher Mn content of the Nb-Ti steel lowered the Ar_3 temperature and, hence, shifted the ductility trough to lower temperatures. Failure at minimum ductility is due to microvoid coalescence in the ferrite film, as suggested by dimpled, intergranular fracture surfaces (Figure 5(a)).

Once the test temperature is high enough to prevent the formation of ferrite, the observed low ductility in single-phase austenite is due to failure by grain boundary sliding. A representative fracture surface, tested at 800 °C, displaying intergranular fracture due to grain boundary sliding is shown in Figure 5(b). The preceding observation is consistent with the Thermo-Calc prediction that the single austenite region extended below 800 °C.

Grain boundary sliding is enhanced by precipitation of fine TiN, Nb(C,N), and NbTi(C,N) in the steels. These findings are in agreement with the well-established notion that fine particles enhance failure by grain boundary sliding[4] and that grain boundary sliding is characterized by intergranular failure with fractographs displaying flat featureless facets.

Previous research has shown that increased cooling rates lead to decreased hot ductility of microalloyed steels due to a refinement of AlN or precipitates containing other alloying elements.[1–3,8,9] The results obtained in the present investigation support, to some extent, this premise in the case of the Nb steel. There was a slight reduction in hot ductility of the Nb steel for specimens tested in the temperature range of 900 °C to 1000 °C when the cooling rate was increased from 100 °C/min to 200 °C/min. This reduction in ductility at higher cooling rates may be related to the fact that finer carbonitrides formed in the steel, which was cooled at a higher rate. The mean carbonitride precipitate size for specimens tested at testing temperatures 950 °C and 900 °C, respectively, were 27.2 and 13.4 nm when a cooling rate of 100 °C/min was used compared to 7.7 and 6.4 nm when a cooling rate of 200 °C/min was used. As shown in Figure 6, there is a sharp drop in ductility when the steel contains particles less than about 15 nm.

There was a sharper drop in hot ductility at a testing temperature of 1000 °C for the Nb-Ti steel at the higher cooling rate. The mean precipitate size at a testing temperature of 1000 °C was 42.8 nm for a cooling rate of 100 °C/min and 23.6 nm for a cooling rate of 200 °C/min. Although this size difference is out of the sensitive range shown in Figure 7, the observed difference in ductility can still be explained by the difference in particle size achieved at the two cooling rates. This finding is of specific practical relevance, because the temperatures of the surface of continuously cast thin slabs are often close to 1000 °C when the strand enters the straightening operation, suggesting a higher propensity for the development of transverse surface cracks.

The hot-ductility curves for specimens cast by pattern I and shown in Figure 2 reveal that the Nb steel has the best hot ductility at temperatures above 900 °C, followed by the Ti steel and then the Nb-Ti steel. The Nb-Ti steel appeared to contain a larger volume fraction of fine precipitates compared to the Ti and Nb steels, and it is suggested that this is the cause of the lower ductility. Volume fractions could not be established quantitatively, and the precipitate density determined from the same number of randomly taken replicas (equal area) was used as a measure to indicate volume fraction. Bright-field TEM micrographs of fine precipitates, extracted onto carbon replicas from specimens tested at 900 °C, for the Nb steel and the Nb-Ti steel are compared in Figure 8. The Nb-Ti steel had a larger particle density presumably because of the presence of both Nb and Ti, which enhance the precipitation of complex carbonitrides as opposed to the formation of binary precipitates.[13,14]

The hot-ductility curves shown in Figure 2 imply that Ti additions to Nb steels will increase the propensity to transverse surface cracking, in agreement with earlier findings in laboratory studies.[7–9,15] On the contrary, industrial practice indicates that small additions of Ti (–0.01 pct) to Nb steel prevents transverse surface cracking in continuous casting practice.[6–10,15] This discrepancy between laboratory tests and commercial experience suggests that laboratory tests fail to accurately simulate conditions during continuous casting, even if specimens for the laboratory tests are cast *in situ*. Mintz[6,10,20] suggested that laboratory tests do not provide a true representation of the influence of Ti additions to steel, because more complex cooling patterns are experienced by continuously cast slabs prior to the straightening operation. The present investigation has indicated that the introduction of thermal oscillations does improve the hot ductility of Nb-Ti steel by influencing the precipitation behaviour, and it is pertinent to further analyze these findings.

The histograms of particle size distributions at a test temperature of 900 °C, shown in Figure 6, show that thermal cycling (pattern II) produces coarser precipitates than the simple pattern I treatment. More specifically, the average precipitate sizes were 30.8, 12.3, and 21.6 nm for cycles 1, 2, and 3, respectively, while average precipitate sizes of 5.2 and 5.8 nm, respectively, were obtained in the case of pattern I treatment at cooling rates of 100 °C/min and 200 °C/min, respectively. The histograms (Figures 6(a) through (c)) for the thermal oscillation tests included large precipitates,

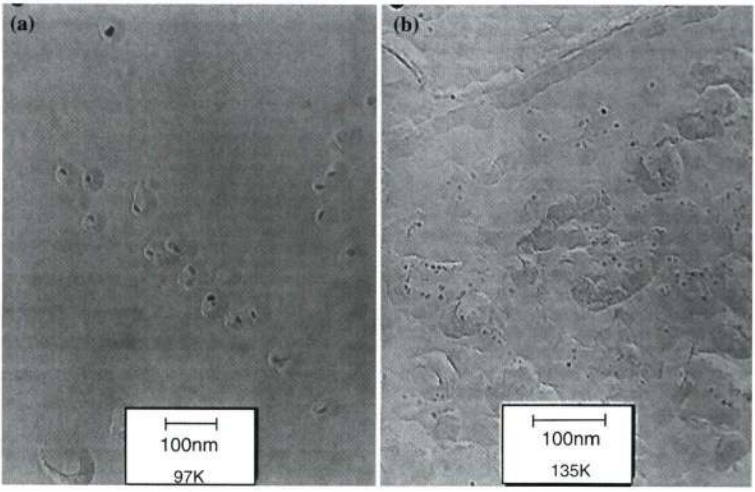

Fig. 8—Bright-field TEM micrographs of fine precipitates on carbon extraction replicas, taken at a test temperature of 900 °C for (*a*) Nb steel and (*b*) Nb-Ti steel.

>40 nm, which were excluded from the average particle size calculations. These large particles were absent in specimens quenched at T_{min} (900 °C), so they were almost certainly formed on reheating from T_{min} to T_{max} (1100 °C).

Increasing the temperature oscillation from ±50 °C (cycle 1) to ±100 °C (cycle 2) resulted in a small decrease in ductility and a smaller average precipitate size. This finding confirms the earlier work by Mintz,[21] where it was found that increasing the amplitude of the temperature cycles enhanced Nb precipitation leading to a wider ductility trough.

Simulation of the complex thermal history of a continuously cast strand under thin-slab casting conditions has shown that the precipitation behavior of NbTi(C,N) in steels that contain both Nb and Ti as alloying elements is influenced by the thermal cycles. The thermal cycles used in the simulation were patterned on the thermal cycles experienced in practice during continuous casting, and it was shown that, under these conditions, precipitation of coarser carbonitride particles is encouraged. In the absence of thermal oscillations, the addition of Ti to a Nb microalloyed steel reduces hot ductility due to the precipitation of fine NbTi(C,N). By contrast, when thermal cycles of the kind described previously are imposed, much coarser carbonitrides precipitate. This finding not only explains the discrepancy between laboratory tests and practical experience (practical experience indicate that Ti additions to Nb-containing steels improve hot ductility whereas laboratory tests indicate a decrease in hot ductility), but it also leads to the important conclusion that conducting hot-ductility tests with an oversimplified cooling pattern leads to erroneous results for microalloyed steels. It is therefore imperative that the complex thermal history experienced by the strand during continuous casting be simulated as closely as possible in the thermal pattern imposed in the hot-ductility test. This will ensure that the precipitation kinetics and evolution experienced in the hot-ductility test represent more closely the events occurring in practice.

V. CONCLUSIONS

1. At low temperatures in the vicinity of the ductility trough, low ductility is attributed to microvoid coalescence within the thin films of ferrite, which form on prior austenite grain boundaries.
2. Reduced ductility at higher temperature is a result of the precipitation of fine carbides, leading to intergranular cracking as a result of grain boundary sliding.
3. This inferior hot ductility of the Nb-Ti steel compared to the simpler Nb- or Ti- containing steels can be related to the enhanced precipitation of NbTi(C,N), making it easier for intergranular cracking to progress by grain boundary sliding.
4. The hot ductility measured in a hot-ductility tensile test is improved if the thermal cycles that the specimen experiences more closely simulate the thermal cycles a strand experiences in practice, because the thermal cycles promote the formation of coarser NbTi(C,N) precipitates.

5. The ability of a tensile hot-ductility test to provide reliable hot-ductility values is significantly improved if the thermal cycles the continuously-cast slab is subjected to are imposed on the specimen during the hot-ductility test.

ACKNOWLEDGMENTS

The authors thank the Australian Research Council and BlueScope Steel for financial support under an ARC-Linkage Grant. Special thanks are due to Mr. Robert De Jong for his assistance with the Gleeble tests and Mr. Greg Tillman for his assistance with metallographic techniques. We also thank Professor Paul Munroe for his assistance with the use of TEM facilities at the UNSW (Sydney, Australia). We thank the University of Wollongong for the provision of laboratory facilities and permission to publish our results.

REFERENCES

1. Y. Maehara, K. Yasumoto, H. Tomono, T. Nagamichi, and Y. Ohmori: *Mater. Sci. Technol.*, 1990, vol. 6 (9), pp. 793–806.
2. R. Abushosha, O. Comineli, and B. Mintz: *Mater. Sci. Technol.*, 1999, vol. 15 (3), pp. 278–86.
3. R. Abushosha, S. Ayyad, and B. Mintz: *Mater. Sci. Technol.*, 1998, vol. 14 (4), pp. 346–51.
4. B. Mintz, S. Yue, and J.J. Jonas: *Int. Mater. Rev.*, 1991, vol. 36 (5), pp. 187–217.
5. B. Mintz and R. Abushosha: *Mater. Sci. Technol.*, 1992, vol. 8 (2), pp. 171–77.
6. B. Mintz: *ISIJ Int.*, 1999, vol. 39 (9), pp. 833–55.
7. R. Abushosha, R. Vipond, and B. Mintz: *Mater. Sci. Technol.*, 1991, vol. 7 (7), pp. 613–21.
8. T.N. Baker: *Titanium Technology in Microalloyed Steels*, The Institute of Materials, London, 1997, pp. 98–113.
9. O. Comineli, R. Abushosha, and B. Mintz: *Mater. Sci. Technol.*, 1999, vol. 15 (9), pp. 1058–68.
10. B. Mintz: *Ironmaking and Steelmaking*, 2000, vol. 27 (5), pp. 343–47.
11. P.A. Manohar and M. Ferry: *Proc. Materials 98*, Biennial Conf. of the Institute of Materials Engineering Australasia, Ltd., Wollongong, Australia, 1988, pp. 131–38.
12. R. Abushosha, R. Vipond, and B. Mintz: *Mater. Sci. Technol.*, 1991, vol. 7 (12), pp. 1101–07.
13. H. Zou and J.S. Kirkaldy: *Metall. Trans. A*, 1991, vol. 22A, pp. 1511–24.
14. S. Okaguchi and T. Hashimoto: *ISIJ Int.*, 1992, vol. 32 (3), pp. 283–90.
15. H. Luo, L.P. Karjalainen, D. Porter, H. Limatainen, and Y. Zhang: *ISIJ Int.*, 2002, vol. 42 (3), pp. 273–82.
16. C.R. Killmore: BlueScope Steel, Port Kembla, Australia, private communication, 2002.
17. B. Mintz: *Mater. Sci. Technol.*, 1996, vol. 12 (2), pp. 132–38.
18. A. Cowley, R. Abushosha, and B. Mintz: *Mater. Sci. Technol.*, 1998, vol. 14 (11), pp. 1145–53.
19. K.W. Andrews: *J. Iron Steel Inst.*, 1965, vol. 203, pp. 721–27.
20. B. Mintz, R. Abushosha, O. Comineli, and S. Ayyad: *Proc. 7th Int. Symp. on Physical Simulation of Casting, Hot Rolling and Welding*, National Research Institute of Japan, Tsukuba, Japan, 1997, pp. 449–59.
21. B. Mintz, J.M. Stewart, and D.N. Crowther: *ISIJ Int.*, 1987, vol. 27, pp. 959–64.